arXiv:1604.03434v4 [nucl-th] 4 Aug 2016

Charge symmetry breaking in the $A = 4$ hypernuclei

Daniel Gazda[a,b], Avraham Gal[c]

[a] *Department of Physics, Chalmers University of Technology, SE-412 96 Göteborg, Sweden*
[b] *Nuclear Physics Institute, 25068 Řež, Czech Republic*
[c] *Racah Institute of Physics, The Hebrew University, 91904 Jerusalem, Israel*

Abstract

Charge symmetry breaking (CSB) in the Λ-nucleon strong interaction generates a charge dependence of Λ separation energies in mirror hypernuclei, which in the case of the $A = 4$ mirror hypernuclei 0^+ ground states is sizable, $\Delta B_\Lambda^{J=0} \equiv B_\Lambda^{J=0}({}^4_\Lambda\mathrm{He}) - B_\Lambda^{J=0}({}^4_\Lambda\mathrm{H}) = 230 \pm 90$ keV, and of opposite sign to that induced by the Coulomb repulsion in light hypernuclei. Recent *ab initio* calculations of the $({}^4_\Lambda\mathrm{H}, {}^4_\Lambda\mathrm{He})$ mirror hypernuclei $0^+_{\mathrm{g.s.}}$ and 1^+_{exc} levels have demonstrated that a $\Lambda - \Sigma^0$ mixing CSB model due to Dalitz and von Hippel (1964) is capable of reproducing this large value of $\Delta B_\Lambda^{J=0}$. These calculations are discussed here with emphasis placed on the leading-order chiral EFT hyperon-nucleon Bonn-Jülich strong-interaction potential model used and the no-core shell-model calculational scheme applied. The role of one-pion exchange in producing sizable CSB level splittings in the $A = 4$ mirror hypernuclei is discussed.

Keywords:
hypernuclei, hyperon-nucleon interactions, charge symmetry breaking

1. Introduction

Charge symmetry breaking (CSB) in the ΛN interaction, which amounts to the difference between the Λn and the Λp interactions, cannot be studied in free space for lack of direct or indirect Λn scattering data and also because none of the two possible $I = \frac{1}{2}$ Λn and Λp systems is bound. Furthermore, it cannot be inferred from the only three-body Λ hypernucleus known to date, the $I = 0$ ${}^3_\Lambda\mathrm{H}$, in which CSB effects are highly suppressed. However, the two four-body $I = \frac{1}{2}$ Λ hypernuclei, ${}^4_\Lambda\mathrm{H}$ with $I_z = -\frac{1}{2}$ and ${}^4_\Lambda\mathrm{He}$ with $I_z = +\frac{1}{2}$,

each one with two particle-stable levels $0^+_{\rm g.s.}$ and $1^+_{\rm exc}$, suggest substantial CSB splitting of the $A = 4$ hypernuclear ground state (see Fig. 1):

$$\Delta B_\Lambda^{J=0} \equiv B_\Lambda^{J=0}({}^4_\Lambda\mathrm{He}) - B_\Lambda^{J=0}({}^4_\Lambda\mathrm{H}) = 233 \pm 92 \text{ keV}. \quad (1)$$

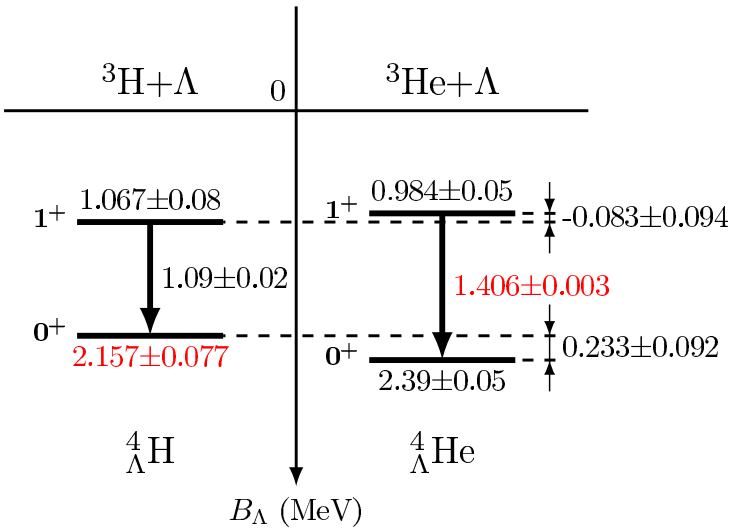

Figure 1: $({}^4_\Lambda\mathrm{H}, {}^4_\Lambda\mathrm{He})$ level diagram (in MeV). The $0^+_{\rm g.s.}$ Λ separation energies B_Λ, loosely termed Λ binding energies, taken from a recent measurement at MAMI [1] for ${}^4_\Lambda$H and from emulsion work [3] for ${}^4_\Lambda$He, are marked under the $0^+_{\rm g.s.}$ energy levels. The $1^+_{\rm exc}$ separation energies follow from γ-ray measurements of the excitation energies E_γ [4] denoted by arrows, and are marked above the $1^+_{\rm exc}$ energy levels. CSB splittings are shown to the right of the ${}^4_\Lambda$He levels. Results from recent measurements are highlighted in red in the online version. Figure adapted from [1].

Until recently, this relatively large observed CSB splitting could not be reproduced in *ab-initio* four-body calculations with the widely used hyperon-nucleon (YN) Nijmegen soft-core meson exchange models $\mathrm{NSC97_{e,f}}$ [5]; see Refs. [6, 7, 8]. A maximal value of $\Delta B_\Lambda^{J=0} \approx 100$ keV was reached in model $\mathrm{NSC97_f}$ [6]. The CSB model used in these past calculations is the $\Lambda - \Sigma^0$ mixing model of Dalitz and von Hippel [9]. In this model, the pure-isospin $I = 0$ $\Lambda^0(uds)$ and $I = 1$ $\Sigma^0(uds)$ octet hyperons which share the $I_z = 0$ central point of the $\mathrm{SU(3)_f}$ octet, as shown in Fig. 2, are admixed by CSB in forming the physical Λ and Σ^0 hyperons. The model relates then the mass-mixing matrix element $\langle\Sigma^0|\delta M|\Lambda\rangle$ to electromagnetic mass differences

of $SU(3)_f$ octet baryons:

$$\langle \Sigma^0 | \delta M | \Lambda \rangle = \frac{1}{\sqrt{3}} \left[(M_{\Sigma^0} - M_{\Sigma^+}) - (M_n - M_p) \right] = 1.143 \pm 0.040 \text{ MeV}. \quad (2)$$

Lattice QCD calculations yield so far only half of this value for the mass-mixing matrix element [10, 11]. The reason apparently is the omission of QED from these calculations [12].

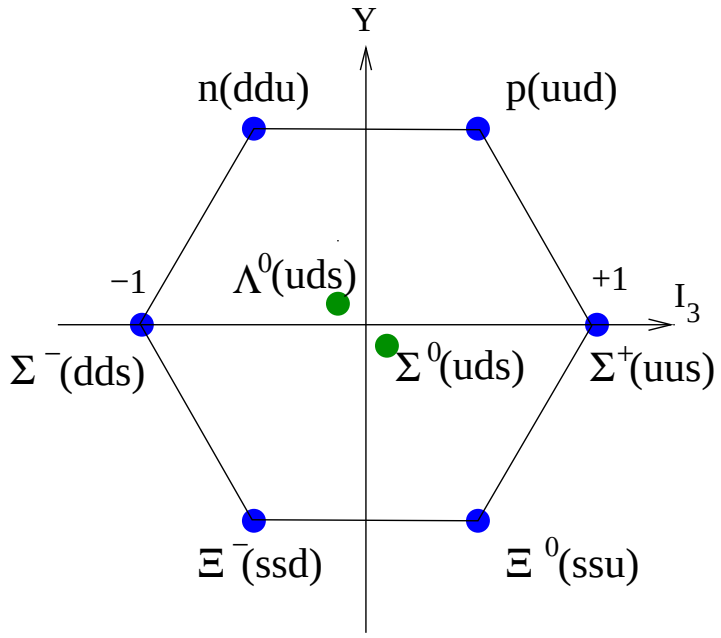

Figure 2: $SU(3)_f$ octet baryons with their underlying leading quark structure. Note the $I = 0$ $\Lambda^0(uds)$ and $I = 1$ $\Sigma^0(uds)$ hyperons, sharing the $I_z = 0$ central point, which are admixed by CSB in the physical Λ and Σ^0 hyperons.

The mass-mixing matrix element (2) serves as insertion in ΛN CSB diagrams generated by the $\Lambda N \leftrightarrow \Sigma N$ strong-interaction (SI) coupling potential $V_{\Lambda N - \Sigma N}$, as shown in Fig. 3, leading to a concrete expression of $V_{\rm CSB}$ ΛN matrix elements in terms of $V_{\rm SI}$ $\Lambda N \leftrightarrow \Sigma N$ matrix elements [13]:

$$\langle N\Lambda | V_{\rm CSB} | N\Lambda \rangle = -0.0297\, \tau_{Nz}\, \frac{1}{\sqrt{3}}\, \langle N\Sigma | V_{\rm SI} | N\Lambda \rangle, \quad (3)$$

where the z component of the isospin Pauli matrix $\vec{\tau}_N$ assumes the values $\tau_{Nz} = \pm 1$ for protons and neutrons, respectively, the isospin Clebsch-Gordan

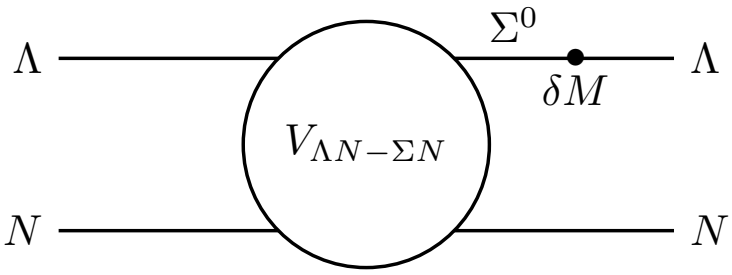

Figure 3: CSB ΛN interaction diagram describing a SI $V_{\Lambda N-\Sigma N}$ interaction followed by a CSB $\Lambda-\Sigma^0$ mass-mixing vertex.

coefficient $1/\sqrt{3}$ accounts for the $N\Sigma^0$ amplitude in the $I_{NY}=\frac{1}{2}$ $N\Sigma$ state, and the space-spin structure of this $N\Sigma$ state is taken identical with that of the $N\Lambda$ state embracing $V_{\rm CSB}$. The CSB scale coefficient 0.0297 in (3) follows from the $\Lambda-\Sigma^0$ mass-mixing matrix element $\langle\Sigma^0|\delta M|\Lambda\rangle$ given above,

$$\frac{2\,\langle\Sigma^0|\delta M|\Lambda\rangle}{M_{\Sigma^0}-M_\Lambda}=0.0297\pm0.0010, \tag{4}$$

where the factor 2 accounts for the two possibilities of inserting δM in Fig. 3, to the left of the SI circle or to its right (as drawn).

Since the charge symmetric SI $\Lambda N\leftrightarrow\Sigma N$ coupling, according to Eq. (3), is the chief provider of the CSB ΛN matrix element, it is natural to ask how strong the $\Lambda N\leftrightarrow\Sigma N$ coupling is in realistic microscopic YN interaction models. In Fig. 4 we show results of no-core shell-model (NCSM) calculations of ${}^{4}_{\Lambda}$He levels [14, 15], using the Bonn-Jülich leading-order (LO) chiral effective field theory (χEFT) YN SI potential model [16], in which $\Lambda N\leftrightarrow\Sigma N$ coupling is seen to contribute between 3 to 4 MeV to the total binding of ${}^{4}_{\Lambda}$He and almost 40% of the $0^+_{\rm g.s.}\rightarrow 1^+_{\rm exc}$ excitation energy $E_{\rm x}$. A similar effect on $E_{\rm x}$ also occurs in the Nijmegen NSC97 models [5]. Recall that in a meson exchange model, one-pion exchange (OPE), forbidden by isospin in the SI ΛN diagonal potential, contributes as strongly as possible to the $\Lambda N\leftrightarrow\Sigma N$ coupling potential. With SI $\Lambda N\leftrightarrow\Sigma N$ potential energy contributions of order 10 MeV [17], and with a CSB scale of order 3%, Eq. (3) could yield CSB contributions of order 300 keV. As shown below, the Bonn-Jülich LO χEFT YN interaction potentials [16] are able to produce this order of magnitude by applying Eq. (3) to each one of the $\Lambda N\leftrightarrow\Sigma N$ $V_{\rm SI}$ components in this LO version. Disregarded in this procedure are CSB

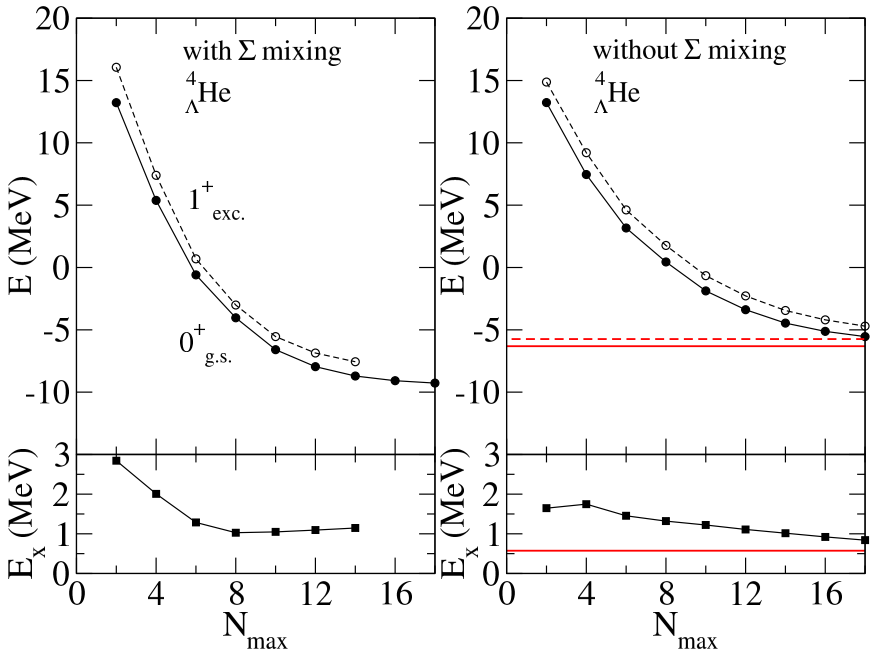

Figure 4: Energy eigenvalues E and excitation energies E_x in NCSM calculations of $^4_\Lambda\mathrm{He}(0^+_{g.s.}, 1^+_{exc})$ states [14, 15] as a function of N_{max}, using LO χEFT YN interactions with cutoff 600 MeV [16], including (left) or excluding (right) $\Lambda\Sigma$ coupling.

contributions arising from meson mixings, such as $\pi^0 - \eta$ and $\rho^0 - \omega$. These were found negligible,

$$\Delta B_\Lambda^{J=0}(\pi^0\eta + \rho^0\omega) \sim -20 \text{ keV}, \quad \Delta B_\Lambda^{J=1}(\pi^0\eta + \rho^0\omega) \sim -10 \text{ keV}, \qquad (5)$$

in four-body ΛNNN calculations by Coon et al. [18] and are disregarded here.[1]

The present work extends our Letter report [20] on CSB level-splitting calculations in the $A = 4$ mirror hypernuclei, adding calculational details, and furthermore comparing the CSB splittings derived from these *ab initio* calculations with those derived by a straightforward evaluation of OPE CSB contributions. The paper is organized as follows: in Sect. 2 we review briefly

[1] In particular, correcting an oversight in Ref. [9], the $\pi^0 - \eta$ mixing contribution to $\Delta B_\Lambda^{J=0}$ is opposite in sign to the positive π^0 exchange contribution from $\Lambda - \Sigma^0$ mixing [19].

the Bonn-Jülich LO χEFT approach followed in our NCSM four-body calculations, as well as providing details of the application of this NCSM technique. Results of these calculations, updating and extending those of Ref. [20], are presented in Sect. 3, with further discussion centered on the role of OPE in Sect. 4. The paper ends with a brief summary and outlook in Sect. 5.

2. Methodology

2.1. NCSM hypernuclear calculations

The version of the NCSM approach which is particularly suitable for dealing with few-body systems employs translationally invariant harmonic-oscillator (HO) bases formulated in relative Jacobi coordinates [21] in which two-body and three-body interaction matrix elements are evaluated. Antisymmetrization is imposed with respect to nucleons, and the resulting Hamiltonian is diagonalized in a finite four-body HO basis, admitting all HO excitation energies $N\hbar\omega$, $N \leq N_{\rm max}$, up to $N_{\rm max}$ HO quanta.

This NCSM nuclear technique was extended recently to light hypernuclei [14, 15] and is applied here in a particle basis, with full account of the different masses within baryon iso-multiplets, to the ${}^{4}_{\Lambda}$H and ${}^{4}_{\Lambda}$He mirror hypernuclei, using momentum-space chiral model interactions specified in Sect. 2.2. Some technical details of the present application of the NCSM methodology to the A=4 mirror hypernuclei are relegated to the unpublished Appendix A. While it was possible to obtain fully converged binding energies, with keV precision, for the A=3 core nuclei ^{3}H and ^{3}He, it was not computationally feasible to perform calculations with sufficiently large $N_{\rm max}$ to demonstrate convergence for ${}^{4}_{\Lambda}$H and ${}^{4}_{\Lambda}$He. In these cases extrapolation to an infinite model space, $N_{\rm max} \to \infty$, had to be employed.[2] Extrapolated energy values $E(\omega)$ are obtained in the present work by fitting an exponential function,

$$E(N_{\rm max}, \omega) = E(\omega) + A\, {\rm e}^{-B\, N_{\rm max}}, \tag{6}$$

with parameters A and B, to $E(N_{\rm max}, \omega$ fixed) sequences in the vicinity of the variational minima with respect to the HO basis frequency ω. The reliability of such extrapolations is then reflected in the independence of $E(\omega)$ of the

[2] The issue of extrapolation in NCSM is unsettled, with somewhat inconclusive discussions of error estimates; see e.g. Refs. [22, 23, 24, 25] and work cited therein for more elaborate methods than the ones employed here.

frequency ω. In our fitting procedure, only the last three $N_{\max}$ values which are the most reliable ones, were used.

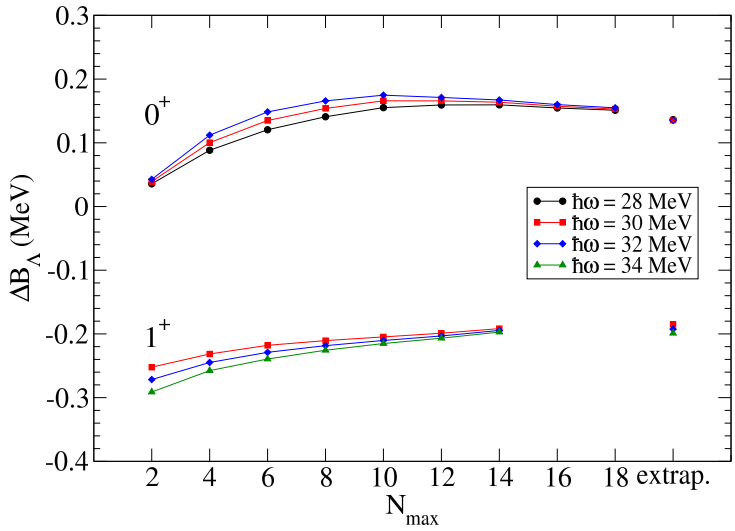

Figure 5: Dependence of the separation-energy differences ΔB_Λ between ${}^{4}_{\Lambda}$He and ${}^{4}_{\Lambda}$H, for $0^+_{\text{g.s.}}$ (upper curves) and for 1^+_{exc} (lower curves) on the model-space size parameter $N_{\max}$ for HO values of $\hbar\omega$ around the variational minima, together with their extrapolated values, in *ab initio* NCSM calculations using LO chiral EFT coupled-channel YN potentials V_{SI}, with cutoff momentum Λ=600 MeV [16], plus V_{CSB} derived from V_{SI} using Eq. (3).

It is worth noting that the present work focuses on *differences* ΔB_Λ of Λ-hyperon separation energies in ${}^{4}_{\Lambda}$H and ${}^{4}_{\Lambda}$He, obtained as

$$\Delta B_\Lambda = [E({}^3\text{He}) - E({}^{4}_{\Lambda}\text{He})] - [E({}^3\text{H}) - E({}^{4}_{\Lambda}\text{H})], \tag{7}$$

where converged energy values of ^{3}H and ^{3}He are used together with extrapolated energy values for ${}^{4}_{\Lambda}$H and ${}^{4}_{\Lambda}$He. In general, the differences ΔB_Λ are much more stable as function of $N_{\max}$ than the absolute energies are. This is demonstrated in Fig. 5 where the dependence of the separation-energy differences ΔB_Λ, for the $0^+_{\text{g.s.}}$ (upper curves) and the 1^+_{exc} (lower curves) states, on the size of the model space is shown for HO frequencies ω around the variational minima of absolute energies at $\hbar\omega = 30(32)$ MeV for J=0(1), together with their extrapolated values. The values of ΔB_Λ exhibit fairly weak $N_{\max}$ and ω dependence compared to the behavior of the absolute energies, and to a lesser extent the behavior of the Λ separation energies, and the

employed extrapolation scheme is found sufficiently robust for our purposes. With regard to the use of $N_{\max} \to \infty$ extrapolated values based on the last three $N_{\max}$ values, it was found that including the last four $N_{\max}$ values in the fit resulted in ΔB_Λ values that differed by $\lesssim 10$ keV.

2.2. LO χEFT YN interaction input

χEFT interactions are used throughout this work, with N3LO NN and N2LO NNN interactions, [26, 27] respectively, both with momentum cutoff $\Lambda = 500$ MeV. For the SI YN coupled-channel potentials $V_{\rm SI}$ we use the Bonn-Jülich SU(3)-based LO χEFT approach [16] plus $V_{\rm CSB}$ evaluated from $V_{\rm SI}$ by using Eq. (3). In principle, the power counting underlying the EFT scheme allows to include two ΛN CSB contact terms, as done in N3LO NN versions to account quantitatively for the charge dependence of the low-energy NN scattering parameters [26, 28]. Given, however, that low-energy Λp cross sections are poorly known and Λn scattering data are unavailable, the corresponding low-energy constants cannot be determined, unless they are fitted to the two CSB splittings $\Delta B_\Lambda^{J=0,1}$ of the $A = 4$ hypernuclear mirror levels, in which case the $A = 4$ CSB calculation reduces to tautology. This unfortunate occurrence cannot be remedied by going from LO to NLO χEFT YN potentials. For this reason, and anticipating that hypernuclear CSB is driven by the relatively long-range OPE, we disregard CSB contact terms.

The χEFT potentials $V_{\rm SI}$ are regularized in momentum space, using the standard choice [6]

$$\langle p'|V_{\rm SI}|p\rangle \to \langle p'|V_{\rm SI}|p\rangle \times \exp(-\frac{p'^4 + p^4}{\Lambda^4}), \tag{8}$$

in order to remove high-energy components of the hadronic fields involved.[3] In LO, $V_{\rm SI}$ consists of regularized pseudoscalar (PS) π, K and η meson exchanges with coupling constants constrained by $\mathrm{SU(3)_f}$, plus five central interaction low-energy constants (also called contact terms) simulating the short range behavior of the YN coupled channel interactions, all of which are regularized according to (8) with a cutoff momentum $\Lambda \geq m_{\rm PS}$, varied from 550

[3] Unfortunately such momentum-space non-local regulators affect also the long-range part of the potentials, as noted recently by Epelbaum et al. [29] who advocated using coordinate-space local regulators.

to 700 MeV. Two of the five contact terms connect ΛN to ΣN in spin-singlet and triplet s-wave channels, and are of special importance for the calculation of CSB splittings. The dominant meson exchange interaction is OPE which couples the ΛN channel exclusively to the $I = \frac{1}{2}$ ΣN channel. K-meson exchange also couples these two YN channels. This LO $V_{\rm SI}$ ($V_{\rm SI}^{\rm LO}$) reproduces reasonably well, with $\chi^2/({\rm d.o.f.}) \approx 1$, the scarce YN low-energy scattering data. It also reproduces the binding energy of ${}^{3}_{\Lambda}$H, with a calculated value $B_\Lambda({}^{3}_{\Lambda}{\rm H})$=110±10 keV for cutoff 600 MeV [15], consistent with experiment (130±50 keV [3]) and with Faddeev calculations reported by Haidenbauer et al. [6]. Isospin conserving matrix elements of $V_{\rm SI}^{\rm LO}$, given in momentum space, are evaluated here in a particle basis with full account of mass differences within baryon iso-multiplets, while isospin breaking I_{NN} $0 \leftrightarrow 1$ and I_{YN} $\frac{1}{2} \leftrightarrow \frac{3}{2}$ transitions are suppressed. The Coulomb interaction between charged baryons (pp, $\Sigma^{\pm}p$) is included.

Calculations consisting of fully converged ^{3}H and ^{3}He binding energies, and (${}^{4}_{\Lambda}$H, ${}^{4}_{\Lambda}$He) $0^{+}_{\rm g.s.}$ and $1^{+}_{\rm exc}$ binding energies extrapolated to infinite model spaces from $N_{\rm max} = 18(14)$ for $J = 0(1)$ are reported in the next section. The calculated binding energies of the core nuclei, 8.482 MeV for ^{3}H and 7.720 MeV for ^{3}He, reproduce very well the known binding energies. The NNN interaction, was excluded from most of the hypernuclear calculations after verifying that, in spite of adding almost 80 keV to the Λ separation energies $B_\Lambda^{J=0}$ and somewhat less to $B_\Lambda^{J=1}$, its inclusion makes a difference of only a few keV for the CSB splittings ΔB_Λ^J in both the $0^{+}_{\rm g.s.}$ and $1^{+}_{\rm exc}$ states.

3. Results

This section is divided to two parts, one in which the explicit CSB potential $V_{\rm CSB}$ of Eq. (3) is excluded, in order to allow comparison with past calculations, and one in which $V_{\rm CSB}$ is generated from the LO χEFT $\Lambda N \leftrightarrow \Sigma N$ strong interactions used here.

3.1. Without explicit CSB

We start by comparing in Table 1 ($0^{+}_{\rm g.s.}$) and Table 2 ($1^{+}_{\rm exc}$) our NCSM calculations to Nogga's Yakubovsky-equations calculations for ${}^{4}_{\Lambda}$H, both using the same LO χEFT YN interactions with no explicit CSB potential $V_{\rm CSB}$, and also to Nogga's recent calculations using NLO [7]. With uncertainties in calculated B_Λ values arising from different NN input in different LO calculations, and also from the suppressed NNN interaction, all of which

are conservatively estimated to be of the order of ∼0.1 MeV, we cite LO results up to the first decimal point.

Table 1: $B_\Lambda^{J=0}({}^4_\Lambda\mathrm{H})$ values calculated in χEFT approaches, without explicit $V_{\rm CSB}$, for various cutoff momenta Λ (in MeV). $\overline{B}_\Lambda^{J=0}({}^4_\Lambda\mathrm{H})$ stands for the mean±spread of these values.

YN chiral model	Λ=550	Λ=600	Λ=650	Λ=700	$\overline{B}_\Lambda^{J=0}({}^4_\Lambda\mathrm{H})$
LO (present)	2.6	2.4	2.2	2.3	2.4±0.2
LO (Nogga [7])	2.6	2.5	2.4	2.4	2.5±0.1
NLO (Nogga [7])	1.52	1.47	1.52	1.61	$1.53^{+0.08}_{-0.06}$

With estimated NCSM $N_{\rm max}\to\infty$ extrapolation uncertainties ±0.1 MeV for $0^+_{\rm g.s.}$, Table 1 demonstrates a very good agreement between the two LO calculations for $0^+_{\rm g.s.}$ over the full range of momentum cutoff Λ values. Both LO calculations exhibit a moderate cutoff dependence, quantified here by giving the spread of the cutoff-dependent $B_\Lambda^{J=0}({}^4_\Lambda\mathrm{H})$ values around their mean value. The mean value in $\overline{B}_\Lambda^{J=0}({}^4_\Lambda\mathrm{H})$ is close to that expected for ${}^4_\Lambda$H once a negative CSB contribution of the order of ∼100 keV is added. It is worth noting that while the cutoff dependence at NLO is remarkably weak, the calculated $B_\Lambda^{J=0}({}^4_\Lambda\mathrm{H})$ values fall substantially below the $0^+_{\rm g.s.}$ experimental separation energy. This could signal a need to introduce YNN three-body terms, as suggested recently by Petschauer et al. [30]. However, as argued by us in the Letter version of this work [20], these terms are unlikely to give rise to additional CSB contributions.

Table 2: $B_\Lambda^{J=1}({}^4_\Lambda\mathrm{H})$ values calculated in χEFT approaches, without explicit $V_{\rm CSB}$, for various cutoff momenta Λ (in MeV). $\overline{B}_\Lambda^{J=1}({}^4_\Lambda\mathrm{H})$ stands for the mean±spread of these values.

YN chiral model	Λ=550	Λ=600	Λ=650	Λ=700	$\overline{B}_\Lambda^{J=1}({}^4_\Lambda\mathrm{H})$
LO (present)	1.7	1.3	0.9	0.5	1.1±0.6
LO (Nogga [7])	1.9	1.5	1.2	1.0	$1.4^{+0.5}_{-0.4}$
NLO (Nogga [7])	0.85	0.73	0.83	0.90	$0.83^{+0.07}_{-0.10}$

Table 2 exhibits a much stronger cutoff dependence of $B_\Lambda^{J=1}({}^4_\Lambda\mathrm{H})$ in both LO calculations. Our NCSM $N_{\rm max}\to\infty$ extrapolation uncertainties, estimated as ±0.5 MeV for the $1^+_{\rm exc}$ state, are considerably larger than for the $0^+_{\rm g.s.}$, reflecting perhaps the weaker binding of the excited state as also noted

in Nogga's work [17]. Given these uncertainties, the table demonstrates, again, a reasonable agreement between the two LO calculations. In contrast, the NLO $B_\Lambda^{J=1}$ values show a very weak cutoff dependence, as weak almost as for the $0^+_{\rm g.s.}$ in NLO, but all of these $B_\Lambda^{J=1}$ values fall considerably below that anticipated from the $1^+_{\rm exc}$ experimental separation energy. This might suggest, again, a need to introduce YNN three-body terms.

Table 3: $E_{\rm x}(0^+_{\rm g.s.} \to 1^+_{\rm exc})$ in ${}^4_\Lambda$H calculated in χEFT approaches without explicit $V_{\rm CSB}$ for various cutoff momenta Λ (in MeV).

YN chiral model	Λ=550	Λ=600	Λ=650	Λ=700	$\overline{E}_{\rm x}({}^4_\Lambda{\rm H})$
LO (present)	0.9	1.1	1.3	1.8	$1.3^{+0.5}_{-0.4}$
LO (Nogga [7])	0.8	1.0	1.1	1.3	1.05±0.25
NLO (Nogga [7])	0.67	0.75	0.69	0.71	0.71±0.04

The underbinding noted above for the NLO results is manifest also upon inspecting the calculated excitation energies $E_{\rm x}(0^+_{\rm g.s.} \to 1^+_{\rm exc})$ listed in Table 3. Whereas both LO calculations reproduce the value of $E_{\rm x}$ expected from experiment, albeit by virtue of the large spread of their Λ dependent $E_{\rm x}$ values, the nearly Λ-independent $E_{\rm x}$ values in NLO are short by roughly 0.4±0.1 MeV of reproducing the value expected from experiment.

Table 4: Cutoff dependence of $A = 4$ hypernuclear mirror-level splittings $\Delta B_\Lambda^J(A = 4)$ (in keV) from *ab initio* NCSM calculations, using LO YN [16] and N3LO NN [26] χEFT strong interactions plus Coulomb interactions, without any explicit $V_{\rm CSB}$. The HO $\hbar\omega$ values used are 32 MeV for cutoffs $\Lambda = 550, 600$ MeV and 34 MeV for $\Lambda = 650, 700$ MeV.

$\Delta B_\Lambda^J(A = 4)$	Λ=550 MeV	Λ=600 MeV	Λ=650 MeV	Λ=700 MeV
$J = 0$ (keV)	−37	−9	+6	+19
$J = 1$ (keV)	−52	−46	−31	−25

Although no explicit CSB potential $V_{\rm CSB}$ was used in the calculations briefed in this subsection, small residual CSB splittings of hypernuclear mirror levels arise, mainly from two sources: (i) the increased repulsive Coulomb energy of ${}^4_\Lambda$He with respect to that of its ^{3}He nuclear core, estimated long ago by Bodmer and Usmani [31] in a Monte-Carlo four-body calculation,

$$\Delta B_\Lambda^{J=0}({\rm Coul}) = -50 \pm 20 \text{ keV}, \quad \Delta B_\Lambda^{J=1}({\rm Coul}) = -25 \pm 15 \text{ keV}, \qquad (9)$$

which for $J = 0$ is of opposite sign to the positive $\Delta B_\Lambda^{J=0}$ observed; and (ii) ΣN intermediate-state mass differences in kinetic energy terms, estimated

by Nogga et al. [32] (see also Table 2 in Ref. [13]) for the $0^+_{\rm g.s.}$ as

$$\Delta B_\Lambda^{J=0}(\Delta M_\Sigma) \sim \frac{2}{3}\,(M_{\Sigma^-} - M_{\Sigma^+})\,P_\Sigma \approx 50 \pm 10 \text{ keV}, \tag{10}$$

where P_Σ is the ΣNNN admixture probability, of the order of 1% in the $0^+_{\rm g.s.}$ and considerably smaller for the $1^+_{\rm exc}$ state. There is substantial cancellation between these two contributions as seen from Table 4 where we list differences $\Delta B_\Lambda^J(A=4)$ of separation energies computed at given values of ω on top or near the absolute variational energy minima from $N_{\rm max} = 18(14)$ output for $J = 0(1)$, using LO χEFT coupled-channel YN potentials [16] with no explicit $V_{\rm CSB}$. The uncertainty associated with the specific choice of ω amounts to few keV at most. Since the ΣNNN admixture probability increases with the cutoff momentum Λ, owing to the small spatial extension of the ΣNNN components of the four-body wave function, the ΣNNN admixture kinetic-energy positive contribution gradually (as function of Λ) takes over the long-range Coulomb potential negative contribution in the $0^+_{\rm g.s.}$, whereas in the $1^+_{\rm exc}$ state it only reduces the magnitude of the latter by about 50%.

3.2. With explicit CSB

Table 5: Cutoff dependence of Λ separation energies B_Λ^J in ${}^4_\Lambda$H and ${}^4_\Lambda$He (all in MeV) from *ab initio* NCSM calculations, using LO YN [16] and N3LO NN [26] χEFT strong interactions plus Coulomb interactions, and $V_{\rm CSB}$ generated by Eq. (3) from $V_{\rm SI}^{\rm LO}$. Experimental values are from Fig. 1.

$B_\Lambda^J({}^4_\Lambda{\rm Z})$	Λ=550	Λ=600	Λ=650	Λ=700	Experiment
$B_\Lambda^{J=0}({}^4_\Lambda{\rm H})$	2.556	2.308	2.121	2.127	2.16±0.08
$B_\Lambda^{J=0}({}^4_\Lambda{\rm He})$	2.586	2.444	2.365	2.423	2.39±0.05
$B_\Lambda^{J=1}({}^4_\Lambda{\rm H})$	1.744	1.359	0.920	0.738	1.07±0.08
$B_\Lambda^{J=1}({}^4_\Lambda{\rm He})$	1.572	1.166	0.683	0.482	0.98±0.05

In Table 5 we show the cutoff dependence of the calculated Λ separation energies $B_\Lambda^J(A=4)$ for the A=4 mirror hypernuclei, obtained from NCSM calculations with LO χEFT coupled-channel YN potentials [16] and $V_{\rm CSB}$ from Eq. (3). The listed values are derived from $N_{\rm max} \to \infty$ extrapolated binding energy values for the ${}^4_\Lambda$He and ${}^4_\Lambda$H $J = 0, 1$ levels at the cutoff-dependent absolute variational minima which are $\hbar\omega(J=0)$=30,30,32,34 MeV and $\hbar\omega(J=1)$=32,32,34,36 MeV for cutoff values Λ=550,600,650,700

MeV, respectively. We note that the spread of $B_\Lambda^J(\hbar\omega)$ values near the absolute variational minimum for a given cutoff momentum is of the order of 30 keV for $J = 0$ and considerably larger, about 150 keV, for $J = 1$; however, as demonstrated in Fig. 5, it is considerably smaller, in fact marginal, for the CSB splittings ΔB_Λ^J which are the main topic of the present work.

The Λ separation energies listed in Table 5 show a moderate cutoff dependence for the $0^+_{\rm g.s.}$ mirror levels and a stronger dependence for the $1^+_{\rm exc.}$ mirror levels, with mean values for their charge-symmetric (CS) averages given by $\overline{B}_\Lambda^{\rm CS}(0^+_{\rm g.s.})=2.37^{+0.20}_{-0.13}$ MeV and $\overline{B}_\Lambda^{\rm CS}(1^+_{\rm exc.})=1.08^{+0.58}_{-0.47}$ MeV comparing well within their spread with the CS-averaged experimental values derived from the last column in the table. Furthermore, considering NCSM $N_{\rm max} \to \infty$ extrapolation uncertainties, our CS-averaged B_Λ values are in fair agreement with those reported in other four-body calculations using CS LO YN χEFT interactions [6, 7, 8, 14, 15].

Table 6: Cutoff dependence of $A = 4$ hypernuclear mirror-level splittings $\Delta B_\Lambda^J(A = 4)$ (in keV) extracted from the B_Λ^J values listed in Table 5. The *ab initio* NCSM calculations that yield these values use LO YN [16] and N3LO NN [26] χEFT interactions plus Coulomb interactions, with $V_{\rm CSB}$ generated by Eq. (3) from the LO SI YN potentials.

$\Delta B_\Lambda^J(A=4)$	Λ=550 MeV	Λ=600 MeV	Λ=650 MeV	Λ=700 MeV
$J = 0$ (keV)	30	136	244	296
$J = 1$ (keV)	-172	-193	-237	-256

The B_Λ^J values listed in Table 5 demonstrate substantial CSB, particularly for the higher values of the cutoff momentum Λ. The derived CSB level splittings ΔB_Λ^J are listed in Table 6. One notes a strong cutoff momentum dependence of $\Delta B_\Lambda^{J=0}$, varying between 30 to 300 keV upon increasing Λ, together with moderate cutoff dependence of $\Delta B_\Lambda^{J=1}$, varying between -170 to -260 keV, just the opposite than for the separation energies B_Λ^J. Note that $\Delta B_\Lambda^{J=0}$ comes out invariably positive, whereas $\Delta B_\Lambda^{J=1}$ is robustly negative. With mean values $\overline{\Delta B}_\Lambda^{J=0}=177^{+119}_{-147}$ keV and $\overline{\Delta B}_\Lambda^{J=1}=-215^{+43}_{-41}$ keV, the mean values $\overline{\Delta B}_\Lambda^J$ satisfy

$$\overline{\Delta B}_\Lambda^{J=1} \approx -\,\overline{\Delta B}_\Lambda^{J=0} < 0. \tag{11}$$

As discussed in our Letter [20], the reason for the opposite signs and approximately equal sizes of the $J = 0, 1$ CSB level splittings is the dominance of the $^1S_0$ contact term (CT) in the SI $\Lambda N \leftrightarrow \Sigma N$ coupling potential of the LO chiral EFT YN Bonn-Jülich approach [16]. The $^3S_1$ CT is completely

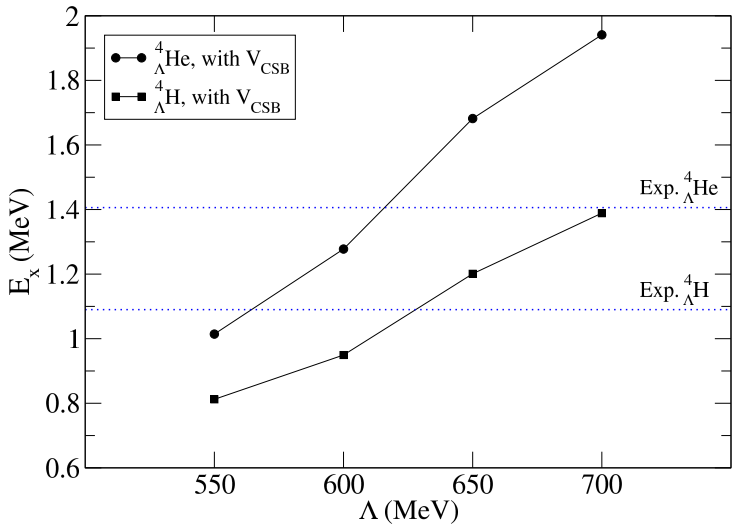

Figure 6: Cutoff momentum dependence of excitation energies $E_{\rm x}(0^+_{\rm g.s.}\to 1^+_{\rm exc})$ in $^4_\Lambda$H (squares; lower curve) and $^4_\Lambda$He (circles; upper curve) in *ab initio* NCSM calculations, at $\hbar\omega$ values yielding absolute variational minima of the total hypernuclear bound-state energy, for LO chiral EFT coupled-channel YN potentials [16] with $V_{\rm CSB}$ derived from these SI potentials using Eq. (3). The dotted horizontal lines denote $E_{\rm x}$ values from γ-ray measurements [4].

negligible in this LO version, whereas the other contributions to ΔB^J_Λ, arising from PS SU(3)-flavor octet ($\mathbf{8}_{\rm f}$) meson exchanges, are relatively small and of opposite sign to that of the $^1S_0$ CT contribution. For $\Lambda = 650$ MeV, for example,

$$\Delta B^{J=0}_\Lambda({\rm CT}) = 313 \text{ keV}, \quad \Delta B^{J=0}_\Lambda(\mathbf{8}_{\rm f}) = -76 \text{ keV}, \tag{12}$$

$$\Delta B^{J=1}_\Lambda({\rm CT}) = -354 \text{ keV}, \quad \Delta B^{J=1}_\Lambda(\mathbf{8}_{\rm f}) = 69 \text{ keV}. \tag{13}$$

Note that the CT and $\mathbf{8}_{\rm f}$ splittings listed here do not add up precisely to the corresponding total values listed in Table 6 owing to the small 'background' CSB contributions surviving in the limit $V_{\rm CSB} \to 0$ (see Table 4) which are present in each one of the listed ΔB^J_Λ values. The small PS $\mathbf{8}_{\rm f}$ meson exchange contributions, including that of the π meson, are opposite in sign to the Dalitz–von Hippel (DvH) OPE contribution [9], which is known to be the strongest meson exchange among the PS $\mathbf{8}_{\rm f}$ meson exchanges. We discuss this puzzling situation in the next section.

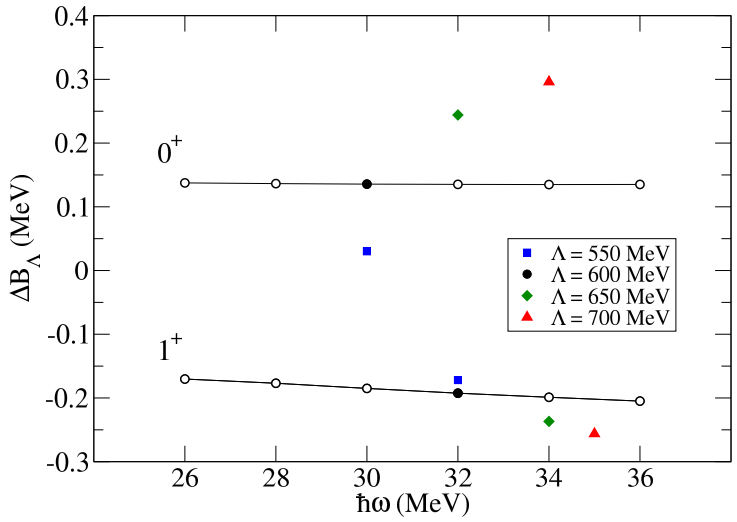

Figure 7: Dependence of the separation-energy differences ΔB_Λ between ${}^{4}_{\Lambda}$He and ${}^{4}_{\Lambda}$H, for $0^+_{\rm g.s.}$ (upper curve) and for $1^+_{\rm exc}$ (lower curve) on the HO $\hbar\omega$ in *ab initio* NCSM calculations using LO chiral EFT coupled-channel YN potentials with cutoff momentum Λ=600 MeV [16] plus $V_{\rm CSB}$ derived from these SI potentials using Eq. (3). Results for other values of Λ are shown at the respective absolute variational energy minima.

The next two figures update two similar ones from our Letter [20] in which the values $\hbar\omega = 30(32)$ MeV for $J = 0(1)$ were used invariably over the full range of values of the cutoff momentum Λ spanned in these figures. The presently used $\hbar\omega$ values are those for the absolute variational energy minima obtained in the NCSM calculations. In Fig. 6 we show by solid lines the cutoff momentum dependence of the $0^+_{\rm g.s.} \to 1^+_{\rm exc}$ excitation energies $E_{\rm x}$ formed from the B_Λ values listed in Table 5 for both A=4 mirror hypernuclei. The dotted horizontal lines mark the values of $E_{\rm x}$ deduced from γ-ray measurements [4]; see Fig. 1. The crossing of these dotted lines with the respective $E_{\rm x}$ solid lines suggests that a choice of cutoff momentum Λ between 600 and 650 MeV gives the best reproduction of $E_{\rm x}$. As noted in several few-body calculations of s-shell hypernuclei [33, 34, 35, 36], and also demonstrated here in Fig. 4, $E_{\rm x}$ is strongly correlated with the $\Lambda N \leftrightarrow \Sigma N$ coupling potential which in the present context, through $\Lambda - \Sigma^0$ mixing, gives rise to CSB splittings of the $A = 4$ mirror levels. One expects then a similarly strong correlation for the CSB splitting of $E_{\rm x}$. Indeed, Fig. 6 shows clearly that as $E_{\rm x}$ increases with Λ, so does the difference $\Delta E_{\rm x} \equiv E_{\rm x}({}^{4}_{\Lambda}{\rm He}) - E_{\rm x}({}^{4}_{\Lambda}{\rm H})$.

In Fig. 7 we show the ω dependence of separation-energy differences ΔB_Λ^J between ${}^4_\Lambda$He and ${}^4_\Lambda$H levels of a given spin J, for $0^+_{\rm g.s.}$ and $1^+_{\rm exc.}$, using $N_{\rm max} \to \infty$ extrapolated values for the four possible binding energies which are calculated for a cutoff Λ=600 MeV and including $V_{\rm CSB}$ from Eq. (3). Extrapolation uncertainties for ΔB_Λ^J are between 10 to 20 keV. The variation of $\Delta B_\Lambda^{J=0}$ in the $\hbar\omega$ range spanned in the figure amounts to a few keV, whereas that of $\Delta B_\Lambda^{J=1}$ is larger, amounting to $\sim$30 keV. It is worth noting that the difference $\Delta B_\Lambda^{J=0} - \Delta B_\Lambda^{J=1}$ between the upper and lower curves assumes at Λ=600 MeV the value 0.33$\pm$0.04 MeV, in perfect agreement with the difference $E_\gamma({}^4_\Lambda{\rm He}) - E_\gamma({}^4_\Lambda{\rm H}) = 0.32 \pm 0.02$ MeV between the two γ ray energies shown in Fig. 1. The figure also shows, again, a strong cutoff dependence of $\Delta B_\Lambda^{J=0}$ together with a moderate cutoff dependence of $\Delta B_\Lambda^{J=1}$.

4. Discussion

Dalitz and von Hippel [9] who suggested the CSB $\Lambda - \Sigma^0$ mass-mixing mechanism, realized its great merit of generating a ΛN OPE long-range CSB potential, $V_{\rm CSB}^{\rm OPE}$, otherwise forbidden by the strong interactions. Disregarding tensor components of OPE, DvH estimated $\Delta B_\Lambda^{J=0}({\rm OPE}) = 165$ keV for the A=4 hypernuclear g.s. Updating some of the relevant coupling constants, their $0^+_{\rm g.s.}$ wave function yields $\Delta B_\Lambda^{J=0}({\rm OPE}) \approx 95$ keV. An exploratory four-body ΛNNN Monte Carlo calculation limited to relative S states by Coon et al. [18] yielded a smaller value of $\Delta B_\Lambda^{J=0}({\rm OPE}) \sim 45$ keV, augmented though by a larger contribution from the very short-ranged ρ meson exchange, $\Delta B_\Lambda^{J=0}({\rm ORE}) \sim 75$ keV. The first $YNNN$ coupled-channel four-body calculation of the A=4 hypernuclei [17, 32], using the coupled-channel YN interaction models NSC97 [5], incorporated OPE and ORE CSB contributions, including those from tensor-interaction components, as well perhaps as other contributions. Surprisingly, small values of $\Delta B_\Lambda^{J=0}$ were found, about 75 keV [32] and 100 keV [6] in versions e and f, respectively, of NSC97.

All of the calculations mentioned above agree in sign, $\Delta B_\Lambda^{J=0}({\rm OPE}) > 0$, with the experimentally derived value of $\Delta B_\Lambda^{J=0}$. However, in the present calculations, a negative OPE contribution is indicated by Eq. (12). To understand this apparent disagreement we list in Tables 7 and 8 partial $V_{\rm CSB}^{\rm OPE}$ contributions to $\Delta B_\Lambda^{J=0}$, computed by adding $V_{\rm CSB}^{\rm OPE}$ directly to the LO χEFT coupled-channel YN potential $V_{\rm SI}$, without activating Eq. (3) which relates $V_{\rm CSB}$ to $V_{\rm SI}$. The SI potentials $V_{\rm SI}$ were regularized by using a cutoff momentum $\Lambda_{\rm SI} = 550$ MeV in Table 7 and $\Lambda_{\rm SI} = 600$ MeV in Table 8, whereas

the momentum-space $V_{\rm CSB}^{\rm OPE}$ was regularized using a sequence of $\Lambda_{\rm CSB}$ values, $\Lambda_{\rm CSB} = 600, 700$ MeV, in each one of the tables. Similarly, results for $\Delta B_\Lambda^{J=1}$(OPE) are listed in Tables 9 and 10 below. We also checked the limit $\Lambda_{\rm CSB} \to \infty$, in which $V_{\rm CSB}^{\rm OPE}$ is not regularized.

Table 7: OPE partial (central and tensor) contributions (in keV) to $\Delta B_\Lambda^{J=0}$ in NCSM A=4 binding energy calculations, using the Bonn-Jülich LO χEFT SI YN potentials [16] with cutoff $\Lambda_{\rm SI} = 550$ MeV. The CSB OPE potential is regularized using cutoff values $\Lambda_{\rm CSB}$ (in MeV). The limiting case $\Lambda_{\rm CSB} \to \infty$ corresponds to unregularized CSB OPE potential. For the meaning of the DvH entries, see text.

$\Lambda_{\rm CSB}$	central	tensor	LO χEFT	central DvH	updated DvH
600	−298	+37	−224	+109	+146
700	−311	+55	−218	+108	+163
$\Lambda_{\rm CSB} \to \infty$	−329	+88	−203	+110	+198

Table 8: Same as Table 7, but for $\Lambda_{\rm SI} = 600$ MeV instead of 550 MeV.

$\Lambda_{\rm CSB}$	central	tensor	LO χEFT	central DvH	updated DvH
600	−264	+81	−167	+102	+183
700	−277	+107	−155	+104	+211
$\Lambda_{\rm CSB} \to \infty$	−297	+158	−124	+106	+264

The OPE potential has two components with contributions listed in the second and third columns: (i) a spin-dependent central component and (ii) a tensor component. These two partial contributions add up approximately, taking into account the 'background CSB' contributions of Table 4 in Sect. 3.1, to the summed OPE contribution in the LO χEFT interaction model given in the fourth column. A spin dependence $\vec{\sigma}_\Lambda \cdot \vec{\sigma}_N$ is responsible for the approximate ratio −3:1 of the $J = 0$ to $J = 1$ central contributions. However, these contributions are of opposite sign to those expected naively from OPE. The resolution of the puzzle is that the central component of this OPE potential, like all PS $\mathbf{8}_{\rm f}$ exchange potentials in the Bonn-Jülich model, consists of two opposite-sign terms which in coordinate space are the familiar Yukawa exponential potential of range m_π^{-1} and a Dirac $\delta(\vec{r})$ zero-range potential. Because both have the same volume integral, the contribution of the $\delta(\vec{r})$ piece is larger in magnitude than the Yukawa contribution, even when smeared by the regularizing form factors, and this is how the sign of the central contribution (second column) in the tables is opposite to what DvH

anticipated. Removing the smeared $\delta(\vec{r})$ term from $V_{\rm CSB}^{\rm OPE}$, one reverses the sign of the central contribution, with the modified central contribution listed in the fifth column under 'central DvH'. As deduced from Tables 7, 8, 9 and 10, this contribution is insensitive to any of the two cutoffs, $\Lambda_{\rm SI}$ and $\Lambda_{\rm CSB}$, within the range of values varied, and the corresponding ≈105 keV contribution for $J = 0$ is consistent with the rough update mentioned above of the DvH central-OPE estimate. In contrast, the tensor contribution, particularly for $J = 0$, is more sensitive to each one of the cutoffs, with a spread of values from the finite $\Lambda_{\rm CSB}$ entries in Tables 7 and 8 given by ∼70±35 keV in the $0^+_{\rm g.s.}$. Altogether the 'updated DvH' total OPE CSB contribution to $\Delta B_\Lambda^{J=0}$ inferred from the finite $\Lambda_{\rm CSB}$ rows is quite large, ∼175±40 keV, with a much smaller-size and negative total OPE CSB contribution, ≈ −48±10 keV, to $\Delta B_\Lambda^{J=1}$. This would fit remarkably well the observed CSB splittings.[4]

Table 9: Same as Table 7, but for $\Delta B_\Lambda^{J=1}$.

$\Lambda_{\rm CSB}$	central	tensor	LO χEFT	central DvH	updated DvH
600	+60	−17	+95	−40	−57
700	+68	−12	+108	−40	−52
$\Lambda_{\rm CSB} \to \infty$	+79	−2	+129	−42	−44

Table 10: Same as Table 8, but for $\Delta B_\Lambda^{J=1}$.

$\Lambda_{\rm CSB}$	central	tensor	LO χEFT	central DvH	updated DvH
600	+73	−4	+109	−39	−43
700	+82	+2	+127	−40	−38
$\Lambda_{\rm CSB} \to \infty$	+96	+15	+151	−42	−27

For the finite values of the cutoff $\Lambda_{\rm CSB}$ listed in Tables 7, 8, 9 and 10, the dependence of the CSB OPE contributions on $\Lambda_{\rm CSB}$ for a given $\Lambda_{\rm SI}$ is weak to moderate, and the limiting case of $\Lambda_{\rm CSB} \to \infty$ poses no convergence problem. However, once $\Lambda_{\rm CSB}$ is increased beyond roughly 700 MeV, the ORE contribution may no longer be ignored, with a $\delta(\vec{r})$-subtracted central contribution that augments the OPE $\delta(\vec{r})$-subtracted central contribution and

[4] If $\Lambda_{\rm SI}$ values of 600 and 650 MeV that are the closest ones to reproducing the observed $E_{\rm x}$ values, see Fig. 6, are used instead, the 'updated DvH' total OPE CSB contribution to $\Delta B_\Lambda^{J=0}$ increases to ∼235±25 keV and that to $\Delta B_\Lambda^{J=1}$ slightly changes to ≈ −35±9 keV.

a tensor contribution that reduces considerably the OPE tensor contribution. We conjecture that the failure of the NSC97 YN models to reproduce the large size of the observed g.s. CSB splitting $\Delta B_\Lambda^{J=0}$ arises from a strong cancellation between the OPE and ORE tensor CSB contributions which in these models overshadow the central CSB contributions.

Finally, the dependence of the total, 'updated DvH' OPE CSB contribution on the strong-interaction cutoff $\Lambda_{\rm SI}$, for a given $\Lambda_{\rm CSB}$, is considerably weaker for the $0^+_{\rm g.s.}$ than that given in Table 6 using Eq. (3) to derive $V_{\rm CSB}$.

5. Summary and outlook

In this work we discussed the extension of the NCSM from few-body nuclear to few-body hypernuclear applications and provided details of our recent Letter publication on *ab initio* calculations of CSB in the A=4 mirror hypernuclei [20]. These calculations are the first microscopic calculations to generate a large positive value of $\Delta B_\Lambda^{J=0}$ commensurate with experiment, although with a considerable momentum-cutoff dependence within the Bonn-Jülich LO χEFT coupled-channel YN potential model [16]. The calculational extrapolation uncertainties involved in the evaluation of $\Delta B_\Lambda^{J=0}$ were estimated to be in the range of 10 to 20 keV at most. In the Bonn-Jülich χEFT approach, the relatively large value derived for $\Delta B_\Lambda^{J=0}$ arises from the $^1S_0$ CT of the SI $\Lambda N \leftrightarrow \Sigma N$ coupling potential, appearing to have no relationship with the large OPE CSB contribution anticipated by DvH [9]. This is a direct consequence of using the relationship given by Eq. (3) between SI and CSB. By removing the short-range $\delta(\vec{r})$ term from the OPE ΛN CSB potential, and using a DWBA-like evaluation of this CSB potential, we were able to recover the DvH original estimate of the central OPE CSB contribution, updated to present-day coupling constants. Furthermore, choosing a cutoff $\Lambda_{\rm SI}$=600 MeV, which is closer to reproducing $E_{\rm x}(0^+_{\rm g.s.} \rightarrow 1^+_{\rm exc})_{\rm exp}$ than the lower cutoff considered here, as large values as $\sim$200 keV for $\Delta B_\Lambda^{J=0}$, and small and negative values ≈ -40 keV for $\Delta B_\Lambda^{J=1}$, emerge for the combined central plus tensor OPE CSB contribution, in striking agreement with experiment. Similar estimates were obtained by one of the authors [13] using a $\Lambda N \leftrightarrow \Sigma N$ effective $V_{\rm SI}$ to which Eq. (3) was applied to generate the corresponding $V_{\rm CSB}$.

Future applications of the NCSM to p-shell hypernuclei are desirable, in view of the few CSB mirror-level splittings known in this mass range [13]. The lesson of this latter work is that genuine CSB splittings become smaller

as one goes to heavier hypernuclei. In this respect, given the particularly large observed value of $\Delta B_{\Lambda}^{J=0}$ in the A=4 mirror hypernuclei considered in the present work, these hypernuclei provide a unique test ground for CSB models beyond nuclear physics.

Appendix A: Jacobi-coordinate NCSM hypernuclear applications

The starting point of the *ab initio* NCSM calculations is the Hamiltonian for a system of nonrelativistic nucleons and hyperons interacting by realistic two-body NN and YN, and also three-nucleon interactions:

$$H = \sum_{i=1}^{A} \frac{\vec{p}_i^{\,2}}{2m_i} + \sum_{i<j=1}^{A} V(\vec{r}_i, \vec{r}_j) + \sum_{i<j<k=1}^{A-1} V(\vec{r}_i, \vec{r}_j, \vec{r}_k). \tag{A.1}$$

In the present work, considering the A=4 mirror hypernuclei, the momenta $\vec{p}_i$, masses m_i and coordinates $\vec{r}_i$ for $i = 1, 2, 3$ correspond to nucleons and those for $i = 4$ to hyperons. The Hamiltonian form (A.1) is then rewritten in terms of *relative* Jacobi coordinates, momenta and their associated masses. There are several different sets of Jacobi coordinates, The first of which is defined by

$$\begin{aligned}
\vec{\xi}_0 &= \sqrt{\frac{1}{M}} \sum_{i=1}^{4} m_i \vec{r}_i, \\
\vec{\xi}_1 &= \sqrt{\frac{m_1 m_2}{m_1 + m_2}} (\vec{r}_1 - \vec{r}_2), \\
\vec{\xi}_2 &= \sqrt{\frac{(m_1 + m_2) m_3}{m_1 + m_2 + m_3}} \left(\frac{m_1 \vec{r}_1 + m_2 \vec{r}_2}{m_1 + m_2} - \vec{r}_3 \right), \\
\vec{\xi}_3 &= \sqrt{\frac{(m_1 + m_2 + m_3) m_4}{M}} \left(\frac{m_1 \vec{r}_1 + m_2 \vec{r}_2 + m_3 \vec{r}_3}{m_1 + m_2 + m_3} - \vec{r}_4 \right),
\end{aligned} \tag{A.2}$$

where $M = \sum_{i=1}^{4} m_i$. This particular set is a natural one for implementing antisymmetrization with respect to nucleons, and is subsequently used for diagonalization of the Hamiltonian. Here, $\vec{\xi}_0$ is proportional to the center of mass coordinate of the A-baryon system and $\vec{\xi}_i$ $(i > 0)$ is proportional to the relative coordinate of the $i + 1$ baryon with respect to the center of mass of

$\leq i$ baryons. The kinetic energy term in Eq. (A.1) is then rewritten in terms of Jacobi cooredinates (A.2):

$$\sum_{i=1}^{4} \frac{\vec{p}_i^{\,2}}{2m_i} \equiv -\sum_{i=1}^{4} \frac{1}{2m_i} \vec{\nabla}^2_{\vec{r}_i} = -\frac{1}{2}\vec{\nabla}^2_{\vec{\xi}_0} - \sum_{i=1}^{3} \frac{1}{2}\vec{\nabla}^2_{\vec{\xi}_i}. \tag{A.3}$$

Since the various interactions V in (A.1) do not depend on $\vec{\xi}_0$, the center of mass kinetic energy can be omitted from (A.3), and one can use an HO basis depending on coordinates $\vec{\xi}_1$, $\vec{\xi}_2$ and $\vec{\xi}_3$, e.g.

$$|((nlsjt)n_3l_3j_3)J_NT_N, n_Yl_Yj_Yt_Y)JT\rangle. \tag{A.4}$$

Here n, l are HO quantum numbers corresponding to coordinate $\vec{\xi}_1$ describing the relative motion of the first two nucleons; n_3, l_3 corresponding to $\vec{\xi}_2$ describe the relative motion of the third nucleon with respect to the nucleon pair; and n_Y, l_Y associated with $\vec{\xi}_3$ describe the relative motion of the hyperon with respect to the three-nucleon cluster. The spin quantum numbers referring to single-particle states are omitted, $s = 0, 1$ is the spin of the two-nucleon pair, and the j quantum numbers denote respective angular momenta. We work in the isospin basis, $t = 0, 1$ is the isospin of the nucleon pair, and the nucleon single-particle isospin is also suppressed in (A.4). The hyperon isospin quantum number $t_Y = 0, 1$ holds for Λ and Σ hyperons, respectively, thereby allowing for explicit admixtures of Σ hyperons into Λ hypernuclear states, induced by the $t_{YN} = \frac{1}{2}$ $\Lambda N \leftrightarrow \Sigma N$ coupling potential. The basis (A.4) is truncated in NCSM calculations by requiring that the total number of HO quanta does not exceed a chosen value $N_{\max}$,

$$2n + l + 2n_3 + l_3 + 2n_Y + l_Y \leq N_{\max} \tag{A.5}$$

thereby defining the size of the model space. Moreover, all HO wave functions in (A.4) depend on a single HO frequency ω which is a free parameter in NCSM calculations.

The basis (A.4) is antisymmetric with respect to exchanging nucleons 1 and 2 upon requiring $(-1)^{l+s+t} = -1$ for the two-nucleon system. It is, however, not antisymmetric with respect to nucleon exchanges $1 \leftrightarrow 3$ and $2 \leftrightarrow 3$. The procedure of fully antisymmetrizing the three-nucleon cluster in the basis (A.4), recalling that it is disconnected from the hyperon quantum numbers, is described in detail e.g. in Ref. [21]. The resulting fully antisymmetric three-nucleon cluster basis elements can be expanded as linear

combinations of the original basis (A.4). Incidentally, the set of coordinates (A.2) is also suitable for evaluating three-nucleon interaction matrix elements which are naturally expressed as functions of the Jacobi coordinates $\vec{\xi}_1$ and $\vec{\xi}_2$ [27].

The basis (A.4) is, however, inappropriate for evaluating two-body interaction terms. Another set of Jacobi coordinates suitable for basis expansion when NN and YN interaction matrix elements are calculated is obtained by keeping to $\vec{\xi}_0$, $\vec{\xi}_1$ and introducing two new variables,

$$\begin{aligned}\vec{\eta}_2 &= \sqrt{\frac{(m_1+m_2)(m_3+m_4)}{M}}\left(\frac{m_1\vec{r}_1+m_2\vec{r}_2}{m_1+m_2}-\frac{m_3\vec{r}_3+m_4\vec{r}_4}{m_3+m_4}\right),\\ \vec{\eta}_3 &= \sqrt{\frac{m_3m_4}{m_3+m_4}}\,(\vec{r}_3-\vec{r}_4)\,.\end{aligned} \tag{A.6}$$

A basis depending on coordinates $\vec{\xi}_1$, $\vec{\eta}_1$, $\vec{\eta}_2$, with two-body subclusters, may be defined e.g. as

$$|((nlsjt),(n_{YN}l_{YN}s_{YN}j_{YN}t_{YN},\mathcal{NL})\mathcal{J})JT\rangle, \tag{A.7}$$

where, similarly to (A.4), the HO state $|nlsjt\rangle$ associated with the coordinate $\vec{\xi}_1$ describes the nucleon pair and the HO state $|n_{YN}l_{YN}s_{YN}j_{YN}t_{YN}\rangle$ associated with $\vec{\eta}_3$ corresponds to the relative-coordinate hyperon–nucleon channel, with $s_{YN}=0,1$, j_{YN} and $t_{YN}=\frac{1}{2},\frac{3}{2}$ standing for the spin, total angular momentum and isospin of the YN pair, respectively. The HO state $|\mathcal{NL}\rangle$ associated with the coordinate $\vec{\eta}_2$ describes the relative motion of the NN and YN clusters. Properties of HO wave functions and Jacobi coordinates allow basis elements defined in (A.4) to be expanded in basis (A.7) as follows:

$$\begin{aligned}&|((nlsjt)n_3l_3j_3)J_NT_N,n_Yl_Yj_Yt_Y)JT\rangle\\ &=\sum \hat{T}_N\hat{t}_{YN}(-1)^{t+\frac{1}{2}+t_Y+T}\begin{Bmatrix}t & \frac{1}{2} & T_N\\ t_Y & T & t_{YN}\end{Bmatrix}\\ &\times\hat{j}_Y\hat{J}_N\hat{L}^2\hat{j}_3\hat{s}_{YN}\hat{\mathcal{J}}\hat{j}_{YN}(-1)^{j+j_3+J_N+J+\mathcal{L}+j_{YN}+l_3+l_Y+s_{YN}}\\ &\times\begin{Bmatrix}l_3 & \frac{1}{2} & j_3\\ l_Y & \frac{1}{2} & j_Y\\ L & s_{YN} & \mathcal{J}\end{Bmatrix}\begin{Bmatrix}j & j_3 & J_N\\ j_Y & J & \mathcal{J}\end{Bmatrix}\begin{Bmatrix}\mathcal{L} & l_{YN} & L\\ s_{YN} & \mathcal{J} & j_{YN}\end{Bmatrix}\\ &\times\langle n_{YN}l_{YN}\mathcal{NL}L|n_Yl_Yn_3l_3L\rangle_{\frac{3m+m_Y}{2m_Y}}\\ &|((nlsjt),(n_{YN}l_{YN}s_{YN}j_{YN}t_{YN},\mathcal{NL})\mathcal{J})JT\rangle,\end{aligned} \tag{A.8}$$

where the orthogonal transformation between the Jacobi coordinates $\vec{\xi}_2, \vec{\xi}_3$ and $\vec{\eta}_2, \vec{\eta}_3$ was employed, and $\langle n_{YN} l_{YN} \mathcal{NL} L | n_Y l_Y n_3 l_3 L \rangle_{\frac{3m+m_Y}{2m_Y}}$ is the general HO bracket for two particles, defined e.g in Ref. [37]. Here, m and m_Y are the nucleon and hyperon ($Y = \Lambda$, Σ) masses defined as

$$m = \frac{m_n + m_p}{2} + \frac{m_n - m_p}{A} M_T, \tag{A.9}$$

$$m_\Sigma = \frac{m_{\Sigma^-} + m_{\Sigma^0} + m_{\Sigma^+}}{3}, \tag{A.10}$$

with m_n, m_p, m_{Σ^-}, m_{Σ^0}, and m_{Σ^+} denoting the masses of the neutron, proton, Σ^-, Σ^0, and Σ^+ hyperons, respectively, and M_T is the projection of the total isospin T, $M_T = \mp\frac{1}{2}$ for $({}^4_\Lambda\mathrm{H}, {}^4_\Lambda\mathrm{He})$ respectively. The transformation (A.8) conserves the total J and T and also, quite importantly, the total number of HO quanta,

$$2n + l + 2n_3 + l_3 + 2n_Y + l_Y = 2n + l + 2n_{YN} + l_{YN} + 2\mathcal{N} + \mathcal{L}. \tag{A.11}$$

Using the expansion (A.8), it is straightforward to evaluate matrix elements of two-body interactions in the basis (A.4),

$$\langle \sum_{i<j=1}^{3} V_{ij} \rangle = 3 \langle V_{NN}(\sqrt{\tfrac{2}{m}} \vec{\xi}_1) \rangle, \tag{A.12}$$

$$\langle \sum_{i=1}^{3} V_{i4} \rangle = 3 \langle V_{YN}(\sqrt{\tfrac{m+m_Y}{m\, m_Y}} \vec{\eta}_3) \rangle, \tag{A.13}$$

where the matrix elements on the right hand sides are diagonal in all quantum numbers of the states (A.7) except for n, l and n_{YN}, l_{YN}, respectively, for isospin conserving interactions. Equally straightforward is the evaluation of two-body interactions defined in momentum space, since transformations analogous to those in (A.2) and (A.6) can be introduced for momenta $\vec{p}_i$ by substituting $\vec{r}_i \to \frac{\vec{p}_i}{m_i}$. Both local and non-local interactions can be accommodated within the NCSM methodology.

Realistic NN and YN interactions are, however, usually defined in the particle basis, not in the isospin basis. To evaluate the corresponding matrix elements of V_{NN} between good-isospin basis states (A.7) we use the following

prescription

$$\begin{aligned}
&\langle (t', t'_{YN}) T M_T | V_{NN} | (t, t_{YN}) T M_T \rangle = \delta_{t't} \delta_{t'_{YN} t_{YN}} \\
&\times \sum \langle t\, m\, t_{YN}\, m_{YN} | T\, M_T \rangle^2 \\
&\times \langle \tfrac{1}{2}\, m'_1\, \tfrac{1}{2}\, m'_2 | t\, m \rangle \langle \tfrac{1}{2}\, m_1\, \tfrac{1}{2}\, m_2 | t\, m \rangle \\
&\times \langle \tfrac{1}{2}\, m'_1, \tfrac{1}{2}\, m'_2 | V_{NN} | \tfrac{1}{2}\, m_1, \tfrac{1}{2}\, m_2 \rangle \\
&\equiv V_{NN}(t; t_{YN}, T, M_T).
\end{aligned} \tag{A.14}$$

Here, only the isospin quantum numbers of states (A.7) are displayed. The basis elements are decomposed via Clebsch–Gordan coefficients and the potential matrix elemets are evaluated between two-nucleon states $|\frac{1}{2}\, m_1, \frac{1}{2}\, m_2\rangle$ with single-nucleon isospin projections $m_1 = \pm\frac{1}{2}$ and $m_2 = \pm\frac{1}{2}$. In this procedure the isospin breaking transitions $t = 0 \leftrightarrow 1$ are suppressed, but the resulting isospin-basis defined NN interaction depends parametrically on the isospin of the YN cluster, as well as on the total isospin and its projection. Similarly, a particle-basis defined YN interaction V_{YN} is evaluated as

$$\begin{aligned}
&\langle (t', t'_{YN}) T M_T | V_{YN} | (t, t_{YN}) T M_T \rangle = \delta_{t't} \delta_{t'_{YN} t_{YN}} \\
&\times \sum \langle t\, m\, t_{YN}\, m_{YN} | T\, M_T \rangle^2 \\
&\times \langle 1\, m'_1\, \tfrac{1}{2}\, m'_2 | t_{YN}\, m_{YN} \rangle \langle 1\, m_1\, \tfrac{1}{2}\, m_2 | t_{YN}\, m_{YN} \rangle \\
&\times \langle 1\, m'_1, \tfrac{1}{2}, m'_2 | V_{YN} | 1\, m_1, \tfrac{1}{2}\, m_2 \rangle \\
&\equiv V_{YN}(t_{YN}; t, T, M_T),
\end{aligned} \tag{A.15}$$

where the potential matrix elements are evaluated between hyperon–nucleon states $|1\, m_1, \frac{1}{2}\, m_2\rangle$ with $m_1 = -1, 0, 1$ and $m_2 = \pm\frac{1}{2}$ the isospin projections of hyperon Y and nucleon N, respectively. Again, the isospin-breaking transitions $t_{YN} = \frac{1}{2} \leftrightarrow \frac{3}{2}$ are suppressed. This procedure gives excellent agreement with particle-basis calculations as demonstrated in Ref. [15]. For the A=3,4 hypernuclear systems, the difference between calculated total energies in particle basis and isospin basis using relations (A.14) and (A.15) was found to be only few keV.

Acknowledgments

We are grateful to Petr Navrátil for helpful advice on extensions of nuclear-physics NCSM codes, to Johann Haidenbauer, and Andreas Nogga for providing us with the input LO EFT YN potentials used in the present work,

and to Nir Barnea, Jiří Mareš and Ulf Meißner for useful discussions on issues related to this work. The research of D.G. was supported by the Granting Agency of the Czech Republic (GACR), Grant No. P203/15/04301S.

References

[1] F. Schulz, et al. (A1 Collaboration), Nucl. Phys. A **954** (2016) 149; see also Ref. [2].

[2] A. Esser, et al. (A1 Collaboration), Phys. Rev. Lett. **114** (2015) 232501.

[3] D.H. Davis, Nucl. Phys. A **754** (2005) 3c.

[4] T.O. Yamamoto, et al. (J-PARC E13 Collaboration), Phys. Rev. Lett. **115** (2015) 222501.

[5] Th.A. Rijken, V.G.J. Stoks, Y. Yamamoto, Phys. Rev. C **59** (1999) 21.

[6] J. Haidenbauer, U.-G. Meißner, A. Nogga, H. Polinder, in *Topics in Strangeness Nuclear Physics*, Lecture Notes in Physics **724**, Eds. P. Bydžovský, J. Mareš, A. Gal (Springer, New York, 2007), pp. 113-140.

[7] A. Nogga, Nucl. Phys. A **914** (2013) 140, and references to earlier works cited therein.

[8] A. Nogga, Few-Body Syst. **55** (2014) 757.

[9] R.H. Dalitz, F. von Hippel, Phys. Lett. **10** (1964) 153.

[10] R. Horsley, et al. (QCDSF-UKQCD Collaboration), Phys. Rev. D **91** (2015) 074512.

[11] A. Gal, Phys. Rev. D **92** (2015) 018501.

[12] R. Horsley, et al. (QCDSF-UKQCD Collaboration), Phys. Rev. D **92** (2015) 018502.

[13] A. Gal, Phys. Lett. B **744** (2015) 352.

[14] D. Gazda, J. Mareš, P. Navrátil, R. Roth, R. Wirth, Few-Body Syst. **55** (2014) 857.

[15] R. Wirth, D. Gazda, P. Navrátil, A. Calci, J. Langhammer, R. Roth, Phys. Rev. Lett. **113** (2014) 192502.

[16] H. Polinder, J. Haidenbauer, U.-G. Meißner, Nucl. Phys. A **779** (2006) 244.

[17] A. Nogga, *Nuclear and hypernuclear three- and four-body bound states*, Ph.D. thesis, Ruhr University, Bochum (2001).

[18] S.A. Coon, H.K. Han, J. Carlson, B.F. Gibson, in *Meson and Light Nuclei '98*, Eds. J. Adam, P. Bydžovský, J. Dobeš, R. Mach, J. Mareš (WS, Singapore, 1999), pp. 407-413, arXiv:nucl-th/9903034.

[19] S.A. Coon, P.C. McNamee, Nucl. Phys. A **322** (1979) 267.

[20] D. Gazda, A. Gal, Phys. Rev. Lett. **116** (2016) 122501.

[21] P. Navrátil, G.P. Kamuntavičius, B.R. Barrett, Phys. Rev. C **61** (2000) 044001.

[22] P. Maris, J.P. Vary, A.M. Shirokov, Phys. Rev. C **79** (2009) 014308.

[23] K.A. Wendt, C. Forssén, T. Papenbrock, D. Sääf, Phys. Rev. C **91** (2015) 061301.

[24] S. Liebig, U.-G. Meißner, A. Nogga, Eur. Phys. J. A **52** (2016) 103.

[25] S.A. Coon, M.K.G. Kruse, Int. J. Mod. Phys. E **25** (2016) 164011.

[26] D.R. Entem, R. Machleidt, Phys. Rev. C **68** (2003) 041001(R).

[27] P. Navrátil, Few-Body Syst. **41** (2007) 117.

[28] E. Epelbaum, W. Glöckle, U.-G. Meißner, Nucl. Phys. A **747** (2005) 362.

[29] E. Epelbaum, H. Krebs, U.-G. Meißner, Eur. Phys. J. A **51** (2015) 53.

[30] S. Petschauer, N. Kaiser, J. Haidenbauer, U.-G. Meißner, W. Weise, Phys. Rev. C **93** (2016) 014001.

[31] A.R. Bodmer, Q.N. Usmani, Phys. Rev. C **31** (1985) 1400.

[32] A. Nogga, H. Kamada, W. Glöckle, Phys. Rev. Lett. **88** (2002) 172501.

[33] B.F. Gibson and D.R. Lehman, Phys. Rev. C **37** (1988) 679.

[34] Y. Akaishi, T. Harada, S. Shinmura, K.S. Myint, Phys. Rev. Lett. **84** (2000) 3539.

[35] E. Hiyama, M. Kamimura, T. Motoba, T. Yamada, Y. Yamamoto, Phys. Rev. C **65** (2001) 011301(R).

[36] H. Nemura, Y. Akaishi, Y. Suzuki, Phys. Rev. Lett. **89** (2002) 142504.

[37] L. Trlifaj, Phys. Rev. C **5** (1972) 1534.